

Stellar mass black hole binaries as ULXs

S. A. Rappaport¹, Ph. Podsiadlowski² and E. P. Fahl³

¹ Department of Physics, MIT 37-602B, 77 Massachusetts Ave, Cambridge, MA 02139 (sar@mit.edu)

² Department of Physics, Oxford University, Oxford, UK (podsi@astro.ox.ac.uk)

³ Chandra Fellow; Harvard-Smithsonian Center for Astrophysics; 60 Garden St., Cambridge, MA 02138 (epfahl@cfa.harvard.edu)

20 March 2024

ABSTRACT

Ultraluminous X-ray sources (ULXs) with $L_x > 10^{39}$ ergs s⁻¹ have been discovered in great numbers in external galaxies with ROSAT, Chandra, and XMM. The central question regarding this important class of sources is whether they represent an extension in the luminosity function of binary X-ray sources containing neutron stars and stellar-mass black holes (BHs), or a new class of objects, e.g., systems containing intermediate-mass black holes (100–1000 M_⊙). We have carried out a theoretical study to test whether a large fraction of the ULXs, especially those in galaxies with recent star formation activity, can be explained with binary systems containing stellar-mass black holes. To this end, we have applied a unique set of binary evolution models for black-hole X-ray binaries, coupled to a binary population synthesis code, to model the ULXs observed in external galaxies. We find that for donor stars with initial masses $> 10 M_{\odot}$ the mass transfer driven by the normal nuclear evolution of the donor star is sufficient to potentially power most ULXs. This is the case during core hydrogen burning and, to an even more pronounced degree, while the donor star ascends the giant branch, though the latter phase lasts only 5% of the main sequence phase. We show that with only a modest violation of the Eddington limit, e.g., a factor of 10, both the numbers and properties of the majority of the ULXs can be reproduced. One of our conclusions is that if stellar-mass black-hole binaries account for a significant fraction of ULXs in star-forming galaxies, then the rate of formation of such systems is $\sim 3 \times 10^{-7}$ yr⁻¹ normalized to a core-collapse supernova rate of 0.01 yr⁻¹.

Key words: accretion, accretion disks | black hole physics | stars: binaries: general | stars: neutron | X-rays: binaries

1 INTRODUCTION

The Chandra X-ray Observatory and the XMM mission have been used to study entire populations of accretion powered binary X-ray sources in external galaxies. At distances exceeding 10 Mpc, the sources that can be studied are limited to the luminous end of the distribution function, e.g., $L_x > 10^{37}$ ergs s⁻¹. The observed sources with L_x up to a few 10^{38} ergs s⁻¹ are very likely closely related to the high- and low-mass X-ray binaries that have been well studied for the past four decades in our own Galaxy and its neighbors. However, the discovery of ultraluminous X-ray sources (ULXs) with Einstein (Fabbiano 1989), ROSAT (Colbert & Ptak 2002; Roberts & Warwick 2000), and ASCA (Makashina et al. 2000) has been greatly extended by Chandra and XMM with their far superior sensitivity (see, e.g., reviews by Fabbiano & White 2004; Colbert & Miller 2004). These sources are typically defined to have $L_x > 10^{39}$ ergs

s⁻¹ (2–10 keV) and have been observed to luminosities as high as a few 10^{40} ergs s⁻¹. A key question which observations of these sources seek to answer is whether the compact object is (1) a neutron star of mass $1.4 M_{\odot}$ or black hole of up to $15 M_{\odot}$ (see, e.g., Tanaka & Lewin 1995; Greiner et al. 2001; Lee et al. 2002; McClintock & Remillard 2004), or (2) a black hole of “intermediate mass”, e.g., 100–1000 M_⊙ (e.g., Colbert & Mushotzky 1999). This is the question we address on theoretical grounds in the current work.

ULXs appear in different types of galaxies, including ellipticals (Angelini, Loewenstein, & Mushotzky 2001; Jeltema et al. 2003) where their luminosities are generally confined to $L_x < 2 \times 10^{39}$ ergs s⁻¹ (Irwin, Bragaglia, & Athey 2004). ULXs, a few with luminosities as high as 5×10^{40} ergs s⁻¹, are especially prevalent in galaxies with starburst activity, including ones that have likely undergone a recent dynamical encounter (e.g., Fabbiano, Zezas, & Murray 2001; Wolter & Trinchieri 2003; Belczynski et al. 2004; Fabbiano & White

2004; Colbert & Miller 2004). Two highly photogenic examples are the Antennae and Cartwheel galaxies. The Antennae galaxies (Fabbiano et al. 2001) include 49 very luminous X-ray sources, 18 of which are classified as ULXs (Zezas et al. 2002), and are likely to be by-products of the star formation triggered by the collision of these galaxies (e.g., Hemquist & Weil 1993). Approximately half of the ULXs in the Antennae are identified with young star-forming regions while the other half have no apparent counterpart (see, e.g., Fabbiano & White 2004). The Cartwheel galaxy reveals a substantial number of resolved as well as some unresolved point sources in a ring coinciding with starburst activity and punctuated by numerous H II regions (Wolter & Trinchieri 2003, 2004; Gao et al. 2003). This ring of star formation is apparently propagating outward at 50 km s^{-1} , and the original disturbance was presumably triggered by the penetration of a smaller galaxy some 5×10^8 years ago. The Chandra sensitivity limit at the distance of the Cartwheel (120 Mpc) is $L_x \sim 5 \times 10^{38} \text{ ergs s}^{-1}$.

The ULXs found in these galaxies and numerous others have been suggested to harbor "intermediate-mass black holes" (IMBHs, e.g., Colbert & Mushotzky 1999). The motivation for this is clear. The Eddington limit for spherically symmetric accretion is given by

$$L_{\text{Edd}} \sim 2.5 \times 10^{38} \frac{M}{M_\odot} (1 + X)^{-1} \text{ ergs s}^{-1}; \quad (1)$$

where M is the mass of the accretor, X is the hydrogen mass fraction in the accreted material, and Thomson scattering is taken to be the dominant source of opacity. The Eddington limit for neutron stars is only $2 \times 10^{38} \text{ ergs s}^{-1}$, though a few accretion-powered X-ray sources have typical persistent luminosities of $5 \text{--} 8 \times 10^{38} \text{ ergs s}^{-1}$ (e.g., Levine et al. 1991, 1993) – not quite in the ULX range. Intermediate-mass black holes, by contrast, would have Eddington luminosities of $10^{40} \text{--} 10^{41} \text{ ergs s}^{-1}$ which nicely cover the ULX range. Moreover, the expected spectra from intermediate-mass black holes accreting substantially below their Eddington limit (as would be the case for most of the ULXs if they were IMBHs), would have low inner-disk temperatures, as is inferred for some of the ULXs (Miller et al. 2003; Miller, Fabian, & Miller 2004a,b; Cropper et al. 2004). However, before invoking a new type of hitherto unobserved object, it is sensible to ascertain whether stellar-mass black holes of mass $5 \text{--} 15 M_\odot$ could explain many or most of the ULXs. The corresponding Eddington limit for these sources is as high as $2 \times 10^{39} \text{ ergs s}^{-1}$, i.e., extends into the low end of the ULX range. Several Galactic black-hole transient X-ray sources have been suspected of exceeding their respective Eddington limits, but the best case may be GRS 1915+105 where the observed L_x has been above $10^{39} \text{ ergs s}^{-1}$ about

30% of the time in daily RXTE ASM averages over the past 8 years (A. Levine, private communication). On rare occasions, and for brief intervals, L_x for GRS 1915+105 can be high as $7 \times 10^{39} \text{ ergs s}^{-1}$ ($2 \text{--} 10 \text{ keV}$; e.g., Greiner et al. 1996), which is a few times greater than the Eddington limit for the $14 M_\odot$ black hole in this system (Greiner et al. 2001). If taken at face value, however, sources with Eddington limited stellar-mass black holes would still fall somewhat short in explaining a significant fraction of the observed ULXs.

A number of ideas have been put forth for ways to circumvent the problem of how $10 M_\odot$ black holes could have apparent L_x values as high as a few $10^{40} \text{ ergs s}^{-1}$. King et al. (2001) suggested that the radiation may be geometrically beamed so that the true value of L_x does not, in fact, exceed the Eddington limit. Kording, Falcke, & Marko (2002) proposed that the apparently super-Eddington ULXs are actually emission from microblazar jets that are relativistically beamed along our line of sight. However, studies of the giant ionization nebulae surrounding a number of the ULXs (Pakull & Mirioni 2003) seem to confirm the full luminosity inferred from the X-ray measurements. Begelman (2002) and Ruszkowski & Begelman (2003) found that in radiation pressure dominated accretion disks super-Eddington accretion rates of a factor of 10 can be achieved due to the existence of a photon-bubble instability in magnetically constrained plasmas. They propose that this instability results in a large fraction of the disk volume being composed of tenuous plasma, while the bulk of the mass is contained in high-density regions. The photons then diffuse out of the disk mostly through the tenuous regions, thereby effectively increasing the Eddington limit. This effect is shown to grow as $M^{1/5}$ and may yield a super-Eddington factor (hereafter "Begelman factor") of 10 in disks around stellar-mass black-hole systems.¹

In the present work we investigate whether most of the ULX population – at least in galaxies with current or recent star formation activity – is consistent with black-hole binaries of conventional mass with only mildly super-Eddington luminosities. In order to carry out this study we combine a unique grid of binary evolution models with a binary population synthesis code to compute theoretical X-ray luminosity functions vs. time after a burst of star formation activity has occurred. We then test how well these calculated results match the observations. To the extent that our models are successful, we can invert the problem and constrain some of the uncertain input physics in binary stellar evolution calculations.

In §2 we describe how the incipient black-hole binaries are generated. We also present a grid of 52 black-hole binary models evolved through the phase of mass transfer onto the black hole, i.e., the X-ray phase. In §3 we discuss how we utilize the population synthesis tools to generate X-ray luminosity functions for black-hole binaries as a function of time since a discrete star formation event. The results are presented as color indices of the evolving luminosity function vs. time, as well as quantitative line plots of the populations vs. X-ray luminosity and vs. time. In §4 we discuss how our results apply to ULXs, particularly those that are being observed in increasingly large numbers in external galaxies with Chandra and XMM.

¹ We note that there are essentially no empirical guidelines available concerning the spectral characteristics of a stellar-mass black hole accreting at such super-Eddington rates. They could quite conceivably mimic the spectrum of a more massive black hole accreting at sub-Eddington rates.

2 BINARY EVOLUTION CALCULATIONS

In our previous study related to ULXs (Podsiadlowski, Rappaport, & Han 2003; hereafter PRH) we developed two separate components of the calculations necessary for a binary population synthesis of these objects. In the first, we started with a very large set of massive primordial binaries and generated a much smaller subset of these that evolved to contain a black hole and relatively unevolved companion star. The product was a set of "incipient" black-hole X-ray binaries with a particular distribution of orbital periods, P_{orb} , donor masses, M_2 , and black-hole masses, M_{BH} , for each of a number of different sets of input assumptions (see, e.g., Fig. 2 of PRH). For this part of the calculation, we employed various "prescriptions", based on single star evolution models for the primary, simple orbital dynamics associated with wind mass loss and transfer, assumptions about the magnitude of the wind mass loss from the primary as well as from the core of the primary after the common envelope, and natal kicks during the core collapse and formation of the black hole. Simple energetic arguments were used to yield the final-to-initial orbital separation during the common-envelope phase wherein the envelope of the primary is ejected. Here we utilized a parameter, α_f , which is the inverse of the binding energy of the primary envelope at the onset of the common-envelope phase in units of $G M_1 M_e / R_1$, where M_1 , M_e and R_1 are the total mass, envelope mass, and radius of the primary, respectively. This parameter strongly affects the final orbital separation after the common-envelope phase, where smaller values of α_f correspond to more tightly bound envelopes, and hence more compact post-common-envelope orbits.

Conventional energetic arguments for the ejection of the common envelope yield the following expression for initial final orbital separation:

$$\frac{\alpha_f}{\alpha_{f, \text{CE}}} = \frac{M_{\text{c}} M_2}{M_1} M_2 + \frac{2 M_e}{\alpha_{f, \text{CE}} r_L} \quad (2)$$

(e.g., Webbink 1985; Dewi & Tauris 2000; Pfahl, Rappaport, & Podsiadlowski 2003), where the subscripts "c", "e", and "L" stand for the progenitor of the black hole, its core, and its envelope, respectively, and "2" is for the progenitor of the "donor star" in the black-hole system. The quantity r_L is the Roche lobe radius of the black-hole progenitor in units of $\alpha_{f, \text{CE}}$ is the fraction of the gravitational binding energy between the secondary and the core of the black-hole progenitor that is used to eject the common envelope, and is defined above. For typically adopted parameter values, $\alpha_{f, \text{CE}} = 0.01$ (e.g., Dewi & Tauris 2000), $\alpha_{f, \text{CE}} = 1$, and $r_L = 0.45$ – 0.6 (for an assumed mass ratio between the black-hole progenitor and the companion in the range of $2:1$ – $15:1$), the second term within the parentheses in eq. (2) dominates over the first. In this case, we find the following simplified expression for $\alpha_f = \alpha_1$:

$$\frac{\alpha_f}{\alpha_{f, \text{CE}}} = \frac{r_L}{2} \frac{M_{\text{c}}}{M_1 M_e} M_2 = 0.005 \frac{M_2}{M} \quad (3)$$

where the leading factor is $r_L = 2$ – $1=4$, while the factor in parentheses involving the black-hole progenitor is 0.020 – $0.002 M^{-1}$ for virtually all of the progenitors we consider. This explains why the large majority of the incipient black-

hole binaries found by PRH resulted from an initially very wide orbit ($P_{\text{orb}} = \text{years}$) when the primary attains radii of 1000 – $2300 R_\odot$ preceding the common-envelope phase in order to avoid a merger between the secondary and the core of the primary.

The final orbital separations (and corresponding orbital periods) after the common envelope depend on the initial orbital separations according to eq. (3). These, in turn, depend upon a number of issues associated with the evolution of massive stars and their wind loss characteristics which were explored in PRH. We expect, however, that the distribution of incipient black-hole binaries in the $P_{\text{orb}} - M_2$ plane will lie largely within an envelope bounded at the top by $P_{\text{orb}, \text{it}} / (a_1 M_2)^{3/2}$ (motivated by eq. [3]), and at the bottom by values of $P_{\text{orb}, \text{fb}}$ that just barely avoid a merger between the core of the black-hole progenitor and the companion star. From the results of PRH (see, e.g., their Figs. 2 & 3) we can fit the following semi-empirical expressions to the regions in the $P_{\text{orb}} - M_2$ plane where the incipient black-hole binaries are located:

$$P_{\text{orb}, \text{it}} = \frac{5}{2} \frac{M_2}{M}^{3/2} d^{3/2} \quad (4)$$

$$P_{\text{orb}, \text{fb}} = \frac{1}{2} \frac{M_2}{M}^{1/4} d^{1/4} \quad (5)$$

for $M_2 > 1 M_\odot$. The expression for the lower limit on P_{orb} results from the radius-mass relation for stars on the main sequence and the functional dependence of the Roche-lobe radius on mass ratio. Furthermore, we find empirically that the lower limit on the donor masses in these incipient systems is given by:

$$M_{2, \text{min}} = \frac{1}{2} M_\odot \quad (6)$$

This expression results from the fact that the product of M_2 must exceed a certain value (see eq. [3]) in order to avoid a merger. A more extensive discussion of the generation of the incipient black-hole X-ray binaries and the relevant references are given in PRH. For other references on this subject see, e.g., King & Kolb (1999); Fryer & Kalogera (2001); Portegies Zwart et al. (1997); and Nelemans & van den Heuvel (2001).

For the second part of the PRH study we calculated a small but unique grid of 19 black-hole binary models evolving through the X-ray phase, i.e., where the donor star transfers mass to the black hole. These calculations are done with a full Henyey stellar evolution code so that at least the behavior of the donor star throughout its mass-transfer phase should be quite accurate and realistic. Nonetheless, there are still a number of uncertainties which involve such issues as whether the Eddington limit is strictly adhered to, and when the mass transfer onto the black hole becomes "transient" in nature; we investigate a number of these issues in this work. In PRH we systematically explored a subset of case A binary evolution models where the donor star is initially unevolved at the time when mass transfer onto the black hole commences. Fourteen of the PRH models were for this early case A binary evolution. A few additional models were computed for cases where hydrogen had been partially depleted (also case A) or completely exhausted (early case B)

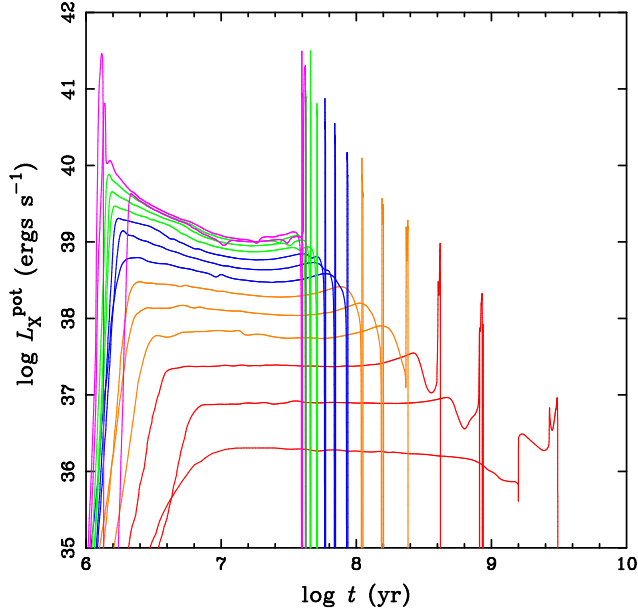


Figure 1. Potential X-ray luminosities as a function of time for 14 black-hole X-ray binary evolution sequences; each color corresponds to a different initial donor star mass ranging from 2 to 17 M_{\odot} (adapted from PRH). The trend in the evolutionary sequences from higher to lower overall X-ray luminosity corresponds to decreasing initial donor mass. In all cases the donor star is unevolved at the start of mass transfer, and the black-hole mass is $10 M_{\odot}$. The spiky feature at the end of each evolution corresponds to the donor star ascending the giant branch. The duration of this latter phase is $\sim 5\%$ of the entire evolution.

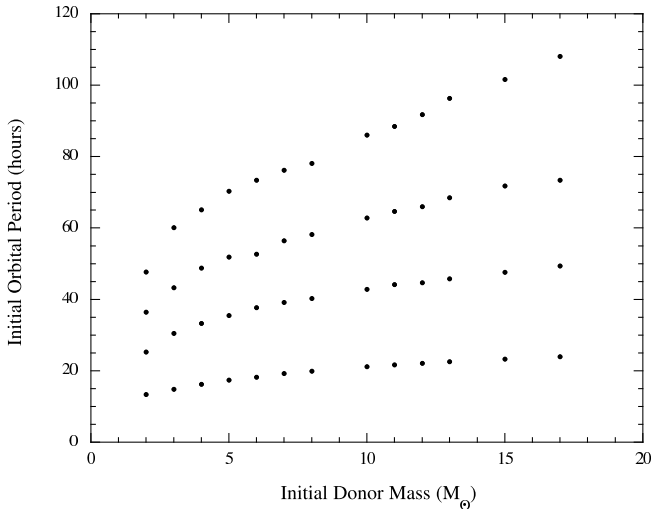


Figure 2. Initial donor masses and orbital periods for the 52 black-hole binary evolution models.

when mass transfer commenced. PRH found that the X-ray lifetime in these latter systems is 1 to 2 orders of magnitude shorter than for systems experiencing case A mass transfer (see Table 1 of PRH and Figs. 3 and 11). Moreover, for large initial mass ratios, mass transfer would be dynamically unstable. We therefore expect that these more evolved systems (cases B and C) will make only a relatively small contribution to the overall population of ULXs.

We reproduce in Fig. 1 plots of the “potential” X-ray luminosity (L_x^{pot}) for 14 binary evolution sequences with initial donor masses of 2 through 17 M_{\odot} from the original models presented in PRH (for the case of initially unevolved donors). The “potential” X-ray luminosity refers to the energy output expected in the absence of the Eddington limit; i.e., if the X-ray luminosity², L_x , were limited only by the mass transfer rate, \dot{M} , and the energy conversion efficiency which is dictated by the instantaneous spin of the black hole (Bardeen 1970). We assumed that each black hole starts with a mass equal to $10 M_{\odot}$ and with zero spin (i.e., $j = 0$, where $0 < j < 1$ is the dimensionless spin parameter). We reiterate that in each model shown in Fig. 1, the donor star is assumed to start on the main sequence when mass transfer commences. We also note that these binary models include, in addition to \dot{M} and L_x , the evolution of P_{orb} , M_2 , M_{BH} , and the spin of the accreting black hole.

In the present work we have significantly augmented our grid of black hole binary evolution models from 19 to 52, and in the process consider case A mass transfer in a more systematic way. The additional models follow the same mass grid as the original 19, except that for each mass we now allow for three additional evolutionary states of the donor star at the onset of mass transfer. This effectively takes into account a significant portion of the expected orbital period distribution among the incipient systems. The different initial evolutionary states of the donor are characterized by the hydrogen mass fraction in the core, X_c . Thus, for each mass, the models are for values of $X_c = 0.7; 0.35; 0.2$; and 0.1 . The corresponding orbital periods at the start of mass transfer range from about 0.6–4 days. The location of the starting points for these models in the M_2 – P_{orb} plane are shown in Fig. 2. To our knowledge, these are the only properly computed evolution models for black-hole binaries during their X-ray phase.

Plots of L_x^{pot} vs. time since the birth of the incipient binary for a sample of our new evolutionary sequences are shown in Fig. 3; these are all for the case where the initial donor mass is $10 M_{\odot}$, but the initial H fraction is different; the black, red, blue, and green curves are for $X_c = 0.7; 0.35; 0.2$; and 0.1 , respectively. Note that, as the donor star is progressively hydrogen depleted at the start of mass transfer, the duration of the mass transfer phase becomes systematically shorter, while the peak values of L_x^{pot} become correspondingly higher. The systematically later times of the onset of mass transfer simply reflect the time that the donor star requires to evolve and fill its Roche lobe. The duration of the main mass-transfer phase becomes shorter, both because the nuclear burning timescale which sets the rate of evolution of the star becomes shorter (and hence leads to a higher mass-transfer rate) and because the remaining core hydrogen-burning lifetime decreases, since less H is available. The rest of the 52 evolutionary sequences are not shown here in the interest of space, but are used in

² Here, as throughout the paper, all calculated luminosities refer to the total accretion luminosity without regard to the region of the X-ray band in which it emerges. Thus, the 2–10 keV luminosity would likely be somewhat lower than the values cited; see x4 for a discussion of this issue.

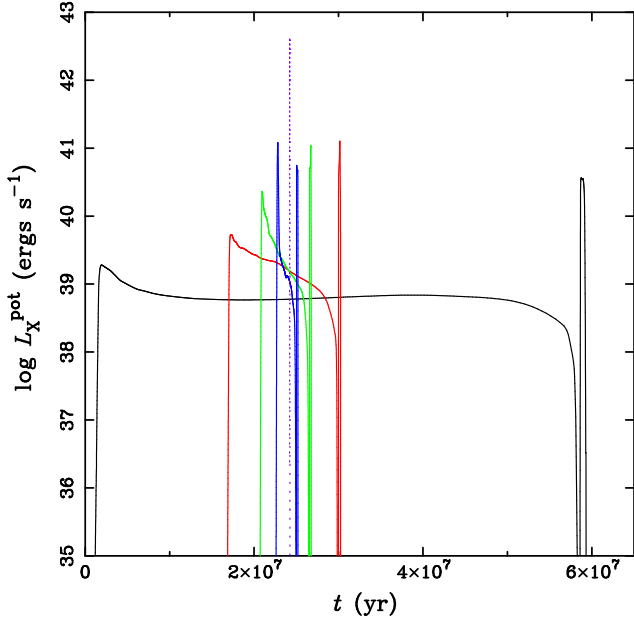


Figure 3. Potential X-ray luminosities as a function of time for 5 black-hole X-ray binary evolution sequences; each color corresponds to a different evolutionary state of the donor star when mass transfer commences. In all cases the initial masses of the donor and black hole are $10M_{\odot}$ and $10M_{\odot}$, respectively. The black, red, green, and blue curves correspond to the central hydrogen abundance of the donor star at the onset of mass transfer of 0.7, 0.35, 0.2, and 0.1, respectively. For comparison, the dotted curve shows the potential X-ray luminosity for a $10M_{\odot}$ secondary that has already evolved off the main sequence (so-called early case B mass transfer), where mass transfer is driven by the expansion of the secondary as it crosses the Hertzsprung gap on a thermal timescale. The duration of the mass-transfer phase is not resolved in the figure, as it lasts only $\sim 50,000$ yr.

the population synthesis study presented in this work, and are available in digital form upon request to the authors.

Experience has shown that population synthesis calculations for systems containing collapsed stars typically require $> 10^4$ systems in order to achieve results of high statistical quality (see, e.g., Howell, Nelson, & Rappaport 2002). Since each of the 52 models we have computed required some half hour of CPU time as well as some hand holding, it is therefore impractical at this time to run thousands of black-hole binary models with a Henyey code to describe the population. However, we have found from our models that the evolutions in L_X form a nearly self-similar set. That is, if we take any two of the evolutionary models, but especially ones that are close in initial M_2 and P_{orb} , then the plots of L_X vs. evolution time can be scaled in time and in L_X so they are nearly the same (see, e.g., Figs. 1 and 3). This is quite different from the case of binary evolution for systems containing neutron stars (see, e.g., Podsiadlowski, Rappaport, & Pfahler 2002) where the evolution tracks for initially similar systems can diverge dramatically. Therefore, we have made use of this self-similar behavior to develop an interpolation scheme to produce an effectively much larger set of models. Thus, if we wish to know the evolution of a binary system starting with values of P_{orb} and M_2 that are within the grid boundaries, but are not located at one of the 52 “nodes”, we

carry out the following variant of a bi-linear interpolation. First, a weighting factor for each of the four nearest grid models (in the P_{orb} – M_2 plane) is computed by linearly interpolating in both P_{orb} and M_2 . Once this has been done, the logarithms of both the beginning and the end times (t_i and t_f) of the four evolutions are interpolated using the weighting factors; this then provides values of $\langle t_i \rangle$ and $\langle t_f \rangle$ to use in the interpolated evolution. Each of the four nearest evolutionary models then has its time axis stretched and shifted so that it begins and ends at $\langle t_i \rangle$ and $\langle t_f \rangle$, respectively. For each time between $\langle t_i \rangle$ and $\langle t_f \rangle$ we then do a logarithmic weighting of the quantity of interest (e.g., L_X) for the four nearest models, using the same weighting factors as described above. We have visually inspected a substantial number of the interpolated evolutions as a check that they behave sensibly.

The black-hole binaries that we produce may account for a significant fraction of the most luminous X-ray sources born in active star forming regions. However, there are several classes of objects not generated in our population synthesis. Not included are the compact black-hole binaries, with low-mass companions, that are transient sources and are observed in abundance in our own Galaxy (see the discussion in PRH). We argue below that these, in fact, may be a separate population and not what is being observed in star formation regions. Moreover, observations of these sources in our own Galaxy indicate that they tend to be limited to $< 10^{38}$ ergs s $^{-1}$, so they may not contribute substantially to the ULX population. We do not consider the evolutionary phase before Roche-lobe overflow when the black hole is fed by accretion from the stellar wind of the companion. Such systems are likely to be at the low end of the luminosity functions we generate in this work, e.g., $10^{34} (M_{BH}/M_{\odot})^2$ ergs s $^{-1}$, where M_{BH} is the mass of the wind-accreting black hole. Also, we do not produce systems where the black hole is formed in very wide primordial binaries without a common envelope being involved, as in the Voss & Tauris (2003) scenario. If objects collapsing to form black holes have natal kicks, and if these kicks are appropriately scaled down by the mass of the collapsed star from the case of neutron star kicks (e.g., to preserve a constant recoil momentum), then the subsequent orbit could fortuitously remain bound and become highly eccentric. Eventually, the donor star would evolve to fill its Roche lobe and mass transfer would then commence. Such systems will, however, tend to have much longer orbital periods than the ones we generate. This has two consequences: (1) many of these will result in unstable mass transfer if the donor star has a mass exceeding that of the black hole; and (2) the mass-transfer phase will be extremely short lived. Finally, we are not considering any systems containing neutron stars since these are not likely to be able to explain the most luminous ULXs. On the other hand, such systems will surely contribute to the luminosity function up to at least $\sim 5 \times 10^{38}$ ergs s $^{-1}$.

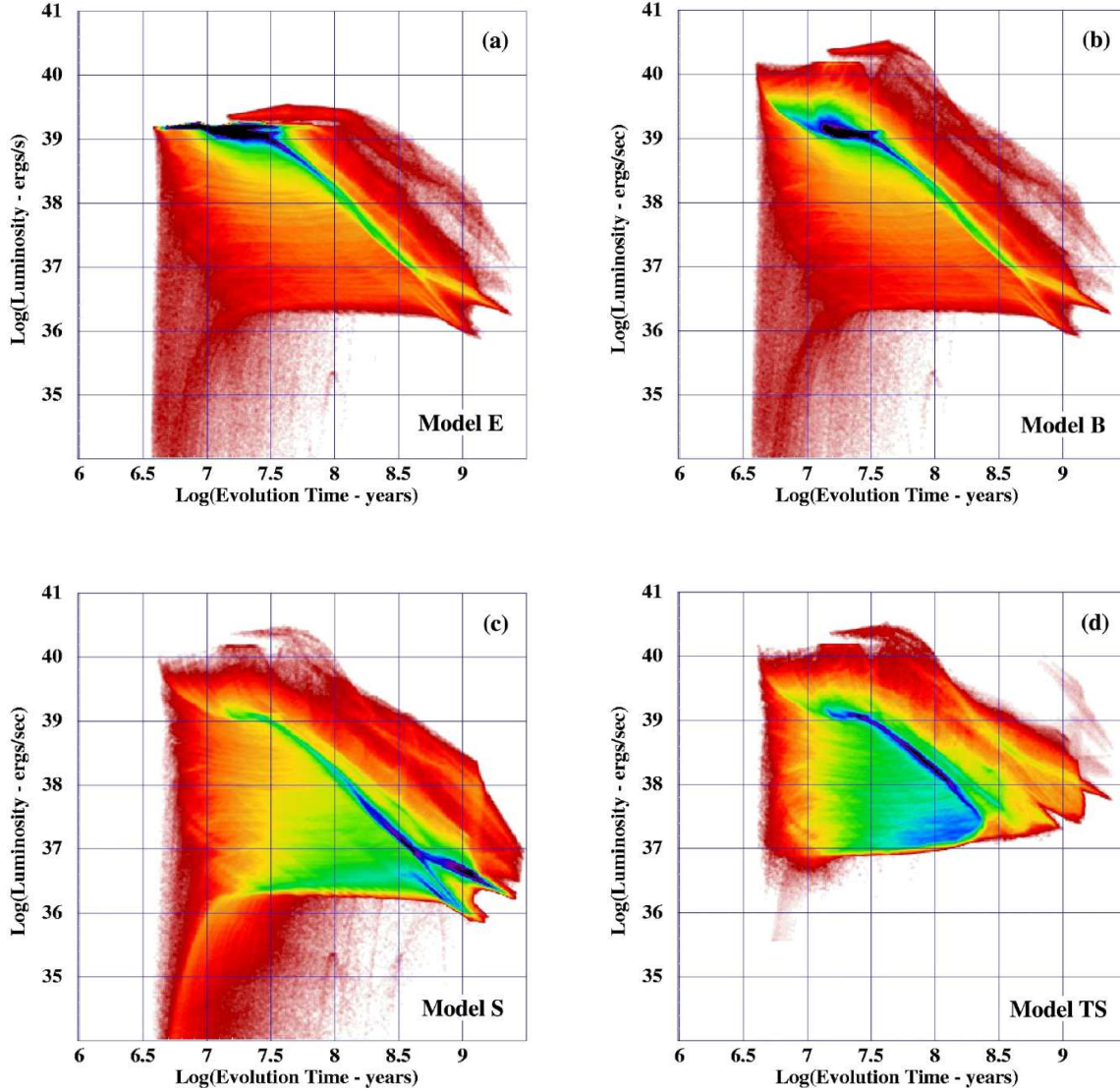


Figure 4. Simulated evolution of the X-ray luminosity function of black hole binaries with time since an impulsive star formation event. "Luminosity" refers to the total accretion luminosity without regard to the region of the X-ray band in which it emerges. Thus, the $2 - 10$ keV luminosity would likely be somewhat lower than the values indicated in the plots. Evolution tracks from 10^6 X-ray sources were computed and then registered in each of the 700×700 pixels that are traversed. The colors crudely represent the logarithm of the relative populations, with purple through red corresponding to ratios of 200 to 1. The mass of the black hole at the start of mass transfer is taken to be $10 M_\odot$. Panel a: Model E. The appropriate Eddington limit of each system has been applied. The upper red bar-like feature between $\log t' = 7.2 - 8.2$ represents systems with donor stars on the giant branch with higher mass transfer rates; the larger black-hole masses later in the evolution and higher He fraction raise L_{Edd} . Panel b: Model B. All specifications are the same as for panel (a), except that the Eddington limit is allowed to be violated by up to a factor of 10 (see text for details), and each system radiates the luminosity that corresponds to the mass transfer rate and the energy conversion efficiency according to the instantaneous spin of the black hole (Bardeen 1970). As in panel (a), the red features at the higher L_x values (at $\log t_{\text{ev}} > 7.2$) are systems with the donor on the giant branch. Panel c: Model S. All specifications are the same as for panel (b), except that the initial mass of the donor star is chosen from a Salpeter initial mass function (Salpeter 1955). This approximates the output from our binary population synthesis code for the case where $\beta = 0.5$. Note that compared to panels (a) & (b) there are many fewer high L_x systems due to the emphasis on the lower-mass donors. Panel d: Model TS. All specifications are the same as for panel (c), except that transient behavior of the X-ray sources is approximately taken into account (see text for details). Such systems are assumed to be in an "on" state only 3% of the time, but with a value of \dot{M} that is 30 times higher than would be the case if the X-ray emission were steady. Note that most of the systems with $L_x < 10^{37}$ ergs s $^{-1}$ no longer appear on the figure, but have been systematically shifted to higher L_x , producing the yellow ridge for main-sequence donors. The faint red feature at times exceeding 10^9 yr with high L_x , corresponds to transients with the donor stars on the giant branch.

3 POPULATION SYNTHESIS CALCULATIONS

We now use the tools described above to generate large populations of black-hole binaries of the type likely to be produced in active star formation regions. The first step is to decide which of the outputs to use from the code that generates the incipient black-hole binaries. Since there are many uncertainties that go into these calculations, we have decided to use somewhat more general distributions of incipient systems in the $P_{\text{orb}} - M_2$ plane that are inspired by the results we found in PRH, rather than taken directly from the specific output for any particular model. We utilize three generic types of distributions for the incipient black-hole binaries. In the first, we take P_{orb} to be uniformly distributed between the two curves given by eqs. (1) and (2), and M_2 to be uniformly distributed between 2 and 17 M_{\odot} . This allows for the broadest contributions from all the binary evolution models that we have calculated, and would directly imply a large value of the parameter β . The second case we consider is one where P_{orb} is distributed uniformly as above, but M_2 is distributed in the same way as the stellar initial mass function as deduced by, e.g., Salpeter (1955), Miller & Scalo (1979), and Kroupa, Tout, & Gilmore (1993). This is a very good approximation to what we find for the high case, e.g., $\beta > 0.5$ (PRH). In this case the envelope of the primary is relatively easy to eject and secondaries over a wide range in mass are able to successfully get past this phase. Their mass distribution then also roughly resembles that of the primaries since we utilize a flat mass ratio distribution (see PRH). The third case we consider is one where β has a small value, e.g., 0.08. In this case only the more massive secondary stars are successful in ejecting the envelope of the primary. For the specific value of $\beta = 0.08$ the incipient population of black-hole binaries has secondary masses largely confined to $M_2 > 6 M_{\odot}$, and the masses are roughly uniformly distributed above this value (see Fig. 2 of PRH).

Throughout this work we have somewhat arbitrarily adopted a fixed black-hole binary production rate of $R_{\text{BH}} \sim 10^{-6} \text{ yr}^{-1}$ and cite a representative value of $\beta \sim 0.1$ in order to normalize all of our luminosity functions. In fact, our earlier binary population synthesis study (hereafter "BPS"; PRH) yielded the following values: $R_{\text{BH}} \sim 10^{-6} \text{ yr}^{-1}$ and $\beta \sim 0.08$ for an incipient black-hole binary population characterized approximately by donor masses uniformly distributed between 6 and 17 M_{\odot} , and $R_{\text{BH}} \sim 3 \times 10^{-6} \text{ yr}^{-1}$ and $\beta \sim 0.5$ for the case where the donor masses are approximately distributed according to the Salpeter (1955) distribution over the mass range 2–17 M_{\odot} . On the other hand, no particular BPS model output corresponded closely to our current choice of a uniform distribution of donor masses between 2 and 17 M_{\odot} , and thus we cannot cite BPS values for R_{BH} and β for this model. In all of our BPS models (PRH) the core-collapse supernova rate was taken to be $R_{\text{SN}} = 10^{-2} \text{ yr}^{-1}$. We comment later in the text on how appropriate we think our adopted rate of 10^{-6} yr^{-1} is for R_{BH} .

In addition to the three different distributions of incipient black hole binaries in the $P_{\text{orb}} - M_2$ plane described above, there are two different assumptions we have made

regarding the maximum X-ray luminosities that can be radiated by a black-hole binary. In the first of these, the maximum value of L_x is taken to be just that given by the Eddington limit which, in turn, is governed by the mass of the black hole and the hydrogen/helium composition of the accreted material. In the second, we allow for the possibility that luminosities up to 10 times the nominal value of L_{Edd} can be attained (Begelman 2002; Ruszkowski & Begelman 2003). Finally, we consider one additional case where the luminosity of the X-ray sources is, under certain physical conditions, transient in its behavior. The transient behavior is thought to arise from the well-known thermal-ionization disk instability (Cannizzo, Gosh, & Wheeler 1982; van Paradijs 1996; King, Kolb, & Burderi 1996; Dubus, Hamury, & Lasota 2001; Lasota 2001). In particular, if the X radiation from the central source is not able to maintain a sufficiently high temperature for the accretion disk (especially for the outer portions), the mass transport through the disk would be unstable, and vice versa. In general, this affects mostly the lower luminosity sources with $L_x < 10^{37} \text{ ergs s}^{-1}$. The specific prescription we used to determine whether a particular model at a given time would exhibit transient behavior is described in detail in PRH (see also x4). When one of our sources is in an evolutionary phase where it would be a transient we simply allow, in a somewhat ad hoc manner, the mass transfer rate onto the black hole to increase by a factor of 30 above the long-term average rate of matter flowing into the disk, but then give that source a probability weighting of only 1/30 in the population, indicating that it would be in an "on" state only 3% of the time. More empirically correct factors to represent transients might be as low as 0.01 for the duty cycle (McIntock & Remillard 2004; and references therein) and up to 100 times the long-term average mass transfer rate. However, as we shall show, transient systems play a relatively minor role in our models of the ULX population, and that would not change even if we had adopted these latter parameters.

In summary, the six models that we have chosen to work with are defined as follows:

Model E is defined to have a uniform incipient population in the $P_{\text{orb}} - M_2$ plane, and the luminosity during the X-ray phase is limited to L_{Edd} ;

Model B is the same, except with a "Begelman" luminosity enhancement such that L_x is permitted to be as large as 10 L_{Edd} ;

Model TB is the same as Model B, but transient source behavior is also included;

Model S is the same as Model B except that M_2 is distributed according to a Salpeter (1955) mass function rather than uniformly in mass;

Model TS is the same as Model S, but transient source behavior is also included;

Model 6 is the same as Model B, except that only values of $M_2 > 6$ are included.

For each of these models we generate a luminosity function vs. time, t_{ev} , since an impulsive star formation event. We choose, via Monte Carlo draws, 10^5 incipient black-hole binaries in the $P_{\text{orb}} - M_2$ plane. To the extent that a particular value of P_{orb} and M_2 lies within our grid of models, we compute an interpolated evolution from the 4 nearest

Table 1. Summary Model Parameters

Name	Model	$N(> 10^{39} \text{ erg s}^{-1})$	$N(> 10^{39.5} \text{ erg s}^{-1})$	$L_{x,\text{tot}}^{(a)}$	$L_{x,\text{tot}}^{(b)}$
E	Eddington limited luminosity	30	0.2	$4 \cdot 10^0$	$1.5 \cdot 10^{+1}$
B	Begelman super Eddington factor	30	6	$6 \cdot 10^0$	$2.3 \cdot 10^{+1}$
TB	Transient behavior included	30	6	$6 \cdot 10^0$	$2.3 \cdot 10^{+1}$
S	Salpeter IMF	4	0.7	$1.0 \cdot 10^0$	$1.5 \cdot 10^{+1}$
TS	Transient behavior included	4	0.7	$1.0 \cdot 10^0$	$1.5 \cdot 10^{+1}$
6	initial donor masses $> 6M$	40	8	$9 \cdot 10^0$	$2.6 \cdot 10^{+1}$

(a) $L_{x,\text{tot}}$ is in units of erg s^{-1} and represents the maximum in the total X-ray luminosity of a galaxy (due to BH-binaries) after a starburst event yielding 10^6 core-collapse SNe. (b) $L_{x,\text{tot}}$ is in units of erg s^{-1} and represents the steady-state total X-ray luminosity of a galaxy (due to BH-binaries) undergoing 0.1 core-collapse SNe per year.

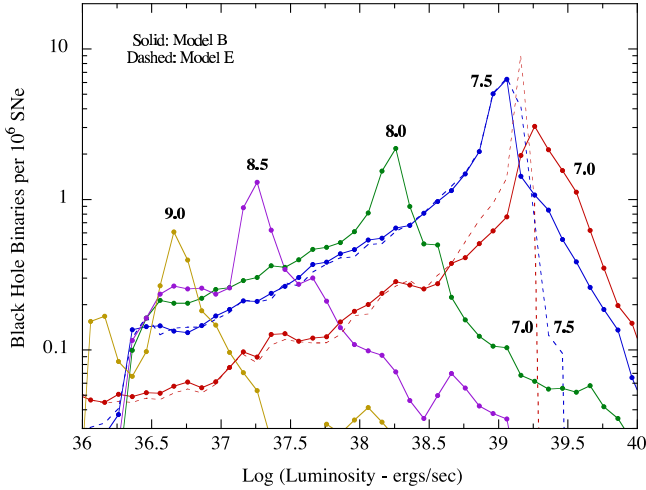


Figure 5. Calculated X-ray luminosity function of black-hole binaries at different epochs after an impulsive star formation event (units are BH-binaries per luminosity bin). The time labels on each curve indicate $\log(t_{\text{ev}})$ in units of years. Solid curves are for Model B (see Fig. 4 (panel b)). The two dashed curves are for Model E (i.e., Eddington limited X-ray luminosities; see Fig. 4 (panel a)) at $\log(t_{\text{ev}}) = 7.0$ and 7.5 ; the curves for all later times are nearly indistinguishable from those of Model B. The distributions are normalized to a star formation event which yielded 10^6 core-collapse SNe.

models, as described in detail in x2. To store the results, we set up an array in the $\log L_x - \log t_{\text{ev}}$ plane, containing 700×700 elements covering the range $10^{34} < L_x < 10^{41} \text{ erg s}^{-1}$ and $10^6 < t_{\text{ev}} < 10^{9.5} \text{ yr}$ in equal logarithmic bins. Each time that one of our evolution tracks crosses an element of this array, a value of unity is added to that element. After this operation has been completed for all 10^5 interpolated evolution tracks, the result is displayed as an image representing the unnormalized evolving luminosity function for each model. These are shown for Models E, B, S, and TS, in Fig. 4. The luminosity function for Models 6 and TB are not shown in the interest of space.

Model E (Fig. 4, panel (a)) shows a large concentration of highly luminous sources ($> 10^{39} \text{ erg s}^{-1}$; i.e., ULXs) at $10 - 30 \text{ Myr}$. These result from systems with the initially more massive companion stars. Between 30 and 300 Myr , the peak in the luminosity function falls monotonically from 10^{39} to $< 10^{37} \text{ erg s}^{-1}$ as systems with the more massive

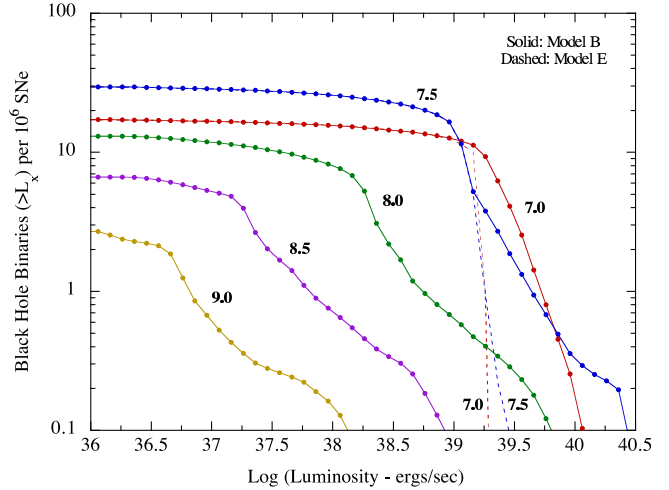


Figure 6. Calculated cumulative X-ray luminosity function of black-hole binaries at different epochs after an impulsive star formation event. The time label on each curve indicates $\log(t_{\text{ev}})$ in units of years. Solid curves are for Model B (see Fig. 4 (panel a)). The two dashed curves are for Model E (i.e., Eddington limited X-ray luminosities; see Fig. 4 (panel a)) at $\log(t_{\text{ev}}) = 7.0$ and 7.5 ; the curves for all later times are nearly indistinguishable from those of Model B. The normalization of the curves is the same as in Fig. 5.

donors run their evolutionary course, leaving longer-lived, lower-luminosity systems with initially lower-mass donors. Numerous systems with L_x exceeding L_{Edd} for a neutron star are still present after 100 Myr . Note the red group of systems at luminosities above the continuous distribution starting at 15 Myr and continuing to $> 1 \text{ Gyr}$; these result from the relatively short-lived phase when the donor stars (of all initial masses) ascend the giant branch and produce mass transfer rates that increase by $1 - 2$ orders of magnitude over the preceding phase of the binary evolution. Finally, note that the apparent upper cutoff in the luminosity function seems to increase by about a factor of 2 for evolution times later than 20 Myr ; this results from the general increase in the black-hole mass as they grow by accretion, and the changing chemical composition of the accreted material which is becoming He enriched.

The evolving luminosity function for Model B (Fig. 4, panel (b)) is very similar to that of Model E, except for the pronounced increase in the allowed upper limit to L_x ,

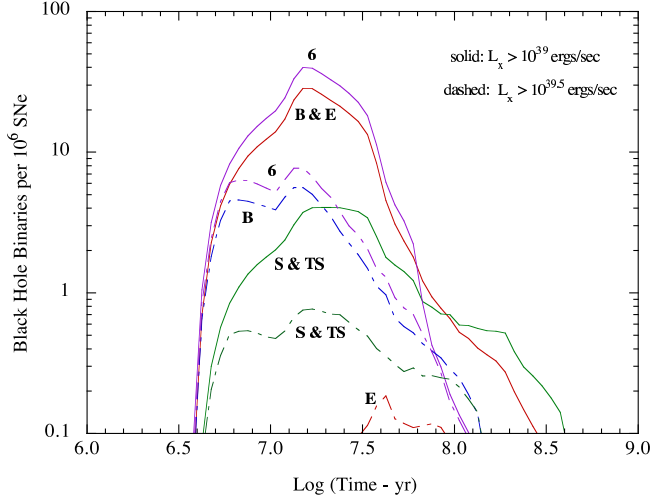


Figure 7. Number of luminous black-hole X-ray binaries as a function of time after an impulsive star formation event. Solid curves represent the number with $L_x > 10^{39}$ ergs s^{-1} ; dashed curves are for $L_x > 3 \times 10^{39}$ ergs s^{-1} . The normalization of the curves is the same as in Fig. 5. The peak value for each curve is listed in Table 1.

by a factor of 10 (as defined by the model). This model allows for a significant population of sources with L_x up to 3×10^{39} ergs s^{-1} and a tailing off population to values of $L_x \sim 2 \times 10^{40}$ ergs s^{-1} for times up to 30 Myr after a star formation event. We note that the luminosity function for Model B (Fig. 4, panel (b)) extends well past the peak in the distribution at all times. Thus, increasing the "Begelem an factor" by more than a factor of 10 would not substantially enhance the population of ULXs.

In Fig. 4, panel (c) we present the evolving luminosity function for Model S, where the initial donor star masses are distributed according to a Salpeter IMF, i.e., with a steeply decreasing population with increasing mass. In such a scenario, the X-ray luminosity function is much less strongly peaked at times < 30 Myr, i.e., not dominated by a narrow range of luminosities, than in the previous models. In particular, there are relatively fewer candidate ULX sources. This is a natural consequence of the smaller numbers of massive donor stars. Finally, the evolving luminosity function for Model TS is presented in Fig. 4, panel (d). In this model, the Salpeter mass distribution is again applied to the incipient donor stars, but transient source behavior due to the thermal/viscous disk instability is now included (in an approximate way). Note that most of the lower luminosity sources (i.e., with $L_x < 10^{37}$ ergs s^{-1}) are missing from the evolving luminosity function. These have been boosted up by a factor of 30 in L_x , but are given a weighting in the "age" of only $1/30$. The effect of the transients is most pronounced for times > 200 Myr where they appear as a yellow ridge in the L_x - t_{ev} plane with L_x in the range of 10^{38} - 10^{39} ergs s^{-1} . Note also the faint red feature appearing at times $> 10^9$ yr which extends into the ULX luminosity range. These are due to donor stars of initially lower mass that are on the giant branch and exhibit transient behavior (GRS 1915+105 in our Galaxy may be an example of such a system).

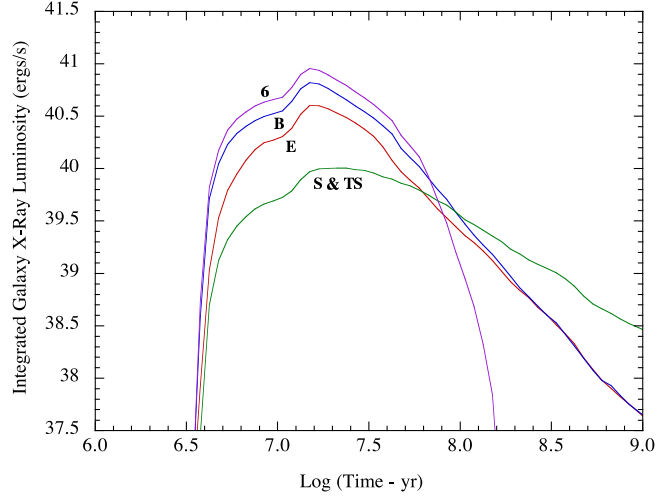


Figure 8. Total luminosity from black-hole X-ray binaries as a function of time after an impulsive star formation event. Results for Models E, B, S, TS, and 6 are shown. The distributions are normalized to a star formation event that yielded 10^6 core-collapse SNe. The peak value for each curve is listed in Table 1.

The evolving luminosity functions presented as in ages are visually informative and interesting, but a somewhat more quantitative way to view these distributions is as one-dimensional plots of either the luminosity functions at specific times or as the evolution with time of the number of sources exceeding a given L_x . The first of these is shown in Fig. 5. Here, the luminosity function is plotted for Model B at 6 different epochs after a star formation event; these are spaced logarithmically every factor of 10 in time, starting at 10^7 yr. Also shown for comparison as a set of dashed lines are luminosity functions for Model E at $\log(t_{ev}) = 7.0$ and 7.5 ; the curves for all later times are nearly indistinguishable from those of Model B. The curves are normalized to 10^6 core-collapse supernovae associated with the star formation event (including those in binary as well as single stars), and to a ratio of the black-hole production rate to that for core-collapse SNe, $R_{BH} = R_{SN}$, equal to 10^{-4} . The most prominent appearance of the ULXs, as could be seen qualitatively in the luminosity function in ages, occurs between 10 and 30 Myr. The same luminosity functions, but plotted as cumulative distributions, are shown in Fig. 6. From this plot it is easy to see that between 10 and 30 Myr a galaxy, undergoing sufficient star formation to produce 10^6 SNe impulsively (e.g., within < 10 Myr), could be expected to harbor more than a dozen ULXs containing stellar-mass black holes. Also, we show in Fig. 7 the number of ULXs ($> 10^{39}$ and $> 10^{39.5}$ ergs s^{-1}) vs. time since a star formation event for Models B, E, S, TS, & 6. These curves have also been normalized to 10^6 SNe and to $R_{BH} = R_{SN} = 10^{-4}$. Finally in this regard, we show in Fig. 8 the integrated X-ray luminosity corresponding to the source numbers given in Fig. 7. Except for Model S, typical integrated X-ray luminosities of 4.9×10^{40} ergs s^{-1} are attained following a large star formation episode (normalized to 10^6 core-collapse SNe).

The type of information contained in the "data" files used to produce Fig. 4 can also be used to construct the

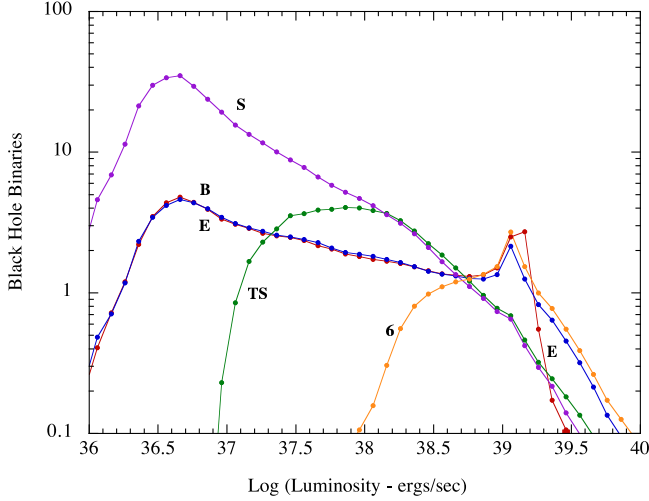


Figure 9. Luminosity functions for a galaxy undergoing continuous star formation at a fixed age 10^8 yr. The core-collapse SN rate is taken to be 0.01 yr^{-1} . The results are derived from Fig. 4 by weighting each column of pixels by the time interval represented by that pixel, and then summing each row of pixels over all columns. Models B, E, S, TS, and 6 are defined in the text.

black-hole binary X-ray luminosity function for any history of star formation. To illustrate this, we compute the luminosity function for a galaxy undergoing continuous, uniform star formation for times exceeding billions of years. To do this we merely sum over the columns of the $L_x - t_{\text{ev}}$ matrix, multiplying each column by its width in time (noting that the widths of the columns increase logarithmically with t_{ev}). The results are shown in Fig. 9 for an assumed formation rate of black-hole binaries of $R_{\text{BH}} = 10^{-6} \text{ yr}^{-1}$ (PRH), which in turn utilizes a SN rate of 0.01 yr^{-1} (e.g., Cappellaro, Evans, & Turatto 1999). The results in Fig. 9, for three of our models (B, E, and 6), indicate that a typical normal spiral galaxy such as our own would have about a half dozen ULXs at any given time. Models S and TS, with a smaller population of initially massive stars, produce of order one ULX, in closer agreement with the observed number in our Galaxy.

We can also use the results of Fig. 9 to compute the integrated X-ray luminosity in the continuous star formation scenario for each of our models. We list the results in Table 1 scaled up by a factor of 10 for better comparison to typical active star-forming galaxies with an assumed core-collapse SN rate of 0.1 yr^{-1} . It is instructive to compare our results with the empirical findings of Gilfanov, Grimmer, & Sunyaev (2004) and Ranalli, Comastri, & Seti (2003) who cite their findings in terms of the relation between the massive star formation rate (SFR), expressed in units of $M_{\odot} \text{ yr}^{-1}$ for stars with $M > 5 M_{\odot}$, and the total X-ray luminosity $L_{\text{X,tot}}$. To intercompare our theoretically derived results with their empirical findings, it is helpful to have a conversion factor between the rate of core-collapse SNe (R_{SN}) and the SFR, which we estimate to be $R_{\text{SN}} \approx 0.025 \text{ SFR}$ for a Salpeter-type IMF. With this conversion we find that our adopted value of $R_{\text{SN}} = 0.1 \text{ yr}^{-1}$ corresponds to an SFR of $4 M_{\odot} \text{ yr}^{-1}$. For this particular value of SFR Gilfanov et

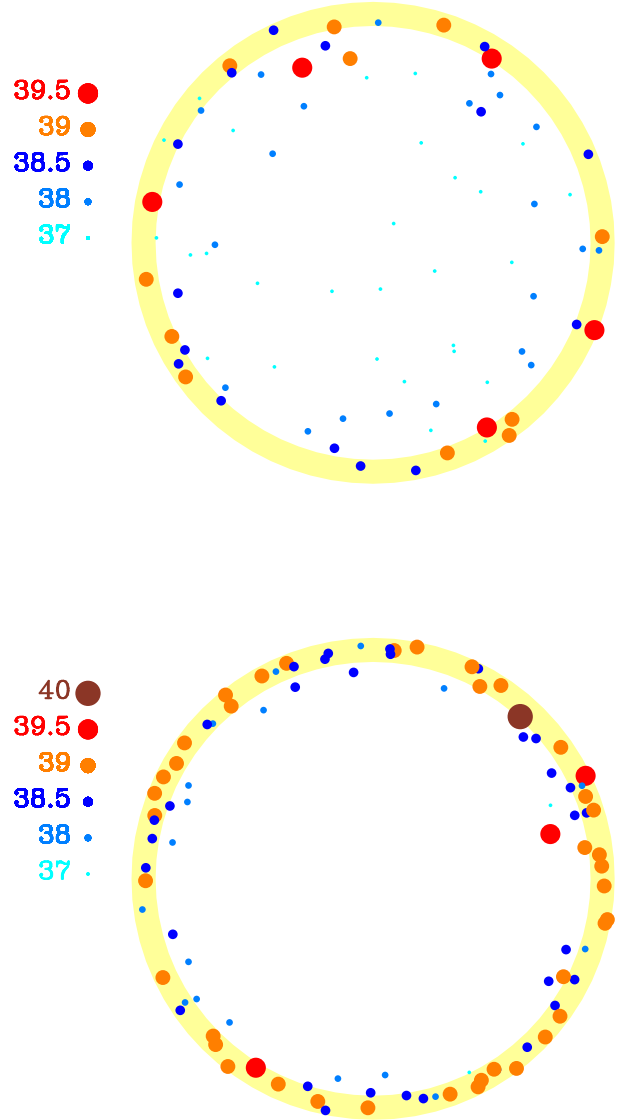


Figure 10. Simulated representation of the luminous black-hole X-ray binaries in a galaxy where a star formation wave was triggered by a catastrophic event at the center some 5×10^8 years ago. The top and bottom panels were produced for Models B and 6, respectively. The wave of star formation is assumed to propagate outward at a constant speed. The surface density of interstellar gas used to form the stars is taken to be a constant per unit surface area. The X-ray luminosities were chosen via a Monte Carlo technique from the distribution for Model B (Fig. 4 (panel b)) and Model 6. This spatial distribution of sources is reminiscent of Chandra images of the Cartwheel galaxy.

al. (2004) and Ranalli et al. (2003) find an average value of $L_{\text{X,tot}} \approx 2 \times 10^{40} \text{ ergs s}^{-1}$. Our tabulated values of $L_{\text{X,tot}}$ (Table 1) for continuous star formation are typically an order of magnitude larger than the empirical value. The values for $L_{\text{X,tot}}$ in Table 1 for impulsive star formation are in better agreement with those of Gilfanov et al. (2004) and Ranalli et al. (2003), but there our normalization of 10^6 core-collapse SNe, which corresponds to, e.g., $R_{\text{SN}} = 0.1 \text{ yr}^{-1}$ for a finite time of 10^7 years, probably underestimates the actual number of SNe contributing to the observed population of luminous X-ray sources. On the other hand, the

assumption of a completely continuous star formation scenario likely overestimates the number of luminous systems. On balance, we conclude that the comparison of our results (Table 1) to those of Gilfanov et al. (2004) and Ranalli et al. (2003) indicates that our adopted formation rate of black-hole binaries of 10^{-6} yr^{-1} for $R_{\text{SN}} = 0.01 \text{ yr}^{-1}$ is likely too high by a factor of ~ 3 . This probably also indicates that our normalization to an effective value of $\beta = 0.1$ (the binding-energy parameter of the BH progenitor) is likely a bit too large; perhaps a better selection would be $\beta = 0.06 - 0.07$.

Finally, we illustrate how, for external galaxies, our results can be used to relate the spatial offsets between ULXs and current star-forming regions. For this we use the evolving luminosity functions after an impulsive star formation event (e.g., Fig. 4). In this exercise we make a crude model for the annular concentration of luminous X-ray sources in the Cartwheel galaxy. We envision an unperturbed spiral galaxy with a uniform surface column density of interstellar gas as the initial condition. We assume that some 5×10^8 years ago a smaller galaxy passed through the center of the spiral and triggered a wave of star formation (Hemquist & Weil 1993) which has just now reached a radius marked by numerous H II regions and luminous X-ray sources. We choose random locations over the surface of the disk (per unit area); the radial distance of each location then specifies the time since the star formation wave has passed. The results shown in Fig. 4, panel (b) are then used as a probability distribution to choose an X-ray luminosity. This is repeated until 100 X-ray sources have been chosen for the realization. The results are shown in the top panel of Fig. 10. The yellow ring marks the outer 10% in radius. Note that while the luminous X-ray sources are indeed concentrated in the outer ring, there are still a number of luminous sources ($> 10^{38} \text{ ergs s}^{-1}$) well inside the ring. We then repeated this exercise for Model 6 where initially more massive donor stars are emphasized; for this model the sources are even more concentrated in the outer 10% of the simulated galaxy (lower panel in Fig. 10).

4 DISCUSSION AND CONCLUSIONS

We have computed a unique grid of 52 black-hole binary evolution models covering donors in the mass range of $2 - 17 M_{\odot}$ and 4 different evolutionary phases at the onset of mass transfer from the ZAMS to the TAMS. We chose the incipient black-hole binaries from regions of the $P_{\text{orb}} - M_2$ plane that were suggestive of the results of the binary population synthesis study by PRH. Several different assumptions were made in choosing the donor masses in the incipient population of black-hole binaries (i.e., Model sets fE, B, TBg, f6g, and fS, TSg). For each incipient binary chosen, we utilized an evolution track that was interpolated from among the binary evolution models in our grid. In this way we computed luminosity functions for large sets of simulated black-hole binaries. The masses of all the black holes in our evolutionary calculations were taken to be initially $10 M_{\odot}$. In future studies the black-hole mass should be taken directly from the population synthesis calculations, and would then range from

$5 - 15 M_{\odot}$ (based on observational constraints; e.g., McClelland & Remillard 2004). The lower black-hole masses,

when paired with the higher-mass donors (e.g., $> 12 M_{\odot}$), would lead to dynamically unstable mass transfer and would then not enter the population. The inclusion of lower-mass black holes will have some modest effect, but certainly not a dominant one, on the luminosity functions that we calculate (see also Fig. 11 and the associated discussion).

Our luminosity functions are sensitive to two principal input parameters. First, the value of β (related to the binding energy of the progenitor of the black hole) directly affects the mass distribution of donor stars in the black-hole binaries. As discussed in the text, there are significant uncertainties in the appropriate values of β to use. The smaller (larger) the value of β the more the incipient donor stars are weighted toward higher (lower) mass. The contributions to the ULX population come from, in decreasing order of importance, black-hole binaries with: (i) high-mass companions, (ii) mid-to high-mass donors on the giant branch, and (iii) lower-mass companions that lead to transient behavior. Second, our results are sensitive to the factor by which we allow for super-Eddington luminosities. In most of our calculations we have used a factor of 10 times the usual values of L_{Edd} (as estimated by Begelman 2002). This substantially helps in the production of ULXs. However, we find that any further increase in this enhancement factor does not significantly increase the number of ULXs since the systems then become limited by the available mass-transfer rates.

We find generally encouraging agreement between the ULX populations that we are able to generate and the observations| at least for the ULX luminosity function below $2 \times 10^{40} \text{ ergs s}^{-1}$. Some of our models, in particular Model B, yield substantial numbers of ULXs for times up to 30 Myr after a star formation event, and a few such sources for times up to 100 Myr. We have found, however, by comparing our production rate of ULXs and the concomitant values of $L_{\text{x,tot}}$ with the empirical relation between the star formation rates and $L_{\text{x,tot}}$ derived by Gilfanov et al. (2004) and Ranalli et al. (2003) that our adopted black-hole binary formation rate of 10^{-6} yr^{-1} for a core-collapse SNe rate of 0.01 yr^{-1} is likely too high by a factor of ~ 3 . Our calculated evolution of the luminosity function after a star formation event can explain spatial offsets between the location of ULXs and current-epoch star-forming regions (e.g., Zezas & Fabbiano 2002; Fabbiano & White 2004, and references therein), provided that the wave of star formation passed from the former to the latter. This is a possible alternative explanation to the one which requires that the ULXs are given natal kicks and ejected from the star clusters in which they are born (e.g., Zezas & Fabbiano 2002).

Throughout this work all of the cited luminosities in the figures and table have been bolometric. On the other hand, most of the literature on ULXs cites L_{x} in the $2 - 10 \text{ keV}$ band due to the sensitivity range of X-ray telescopes. It is difficult to estimate what fraction, f , of the bolometric X-ray luminosity emerges in the $2 - 10 \text{ keV}$ band precisely because very few measurements extend to substantially lower or higher energies. Notwithstanding this limitation, we have used various spectral shapes for ULXs reported in the literature to estimate f . We find values of f between 0.1 and 0.5 with a most probable value of ~ 0.3 . This range for f should hold unless a large fraction of the luminosity is emitted in a

low-temperature multi-component disk spectrum that falls largely outside the 2–10 keV range. (For a related discussion see Appendix A.2 of Portegies Zwart, Dewi, & Maccarone 2004.) We can foresee two distinct possibilities for the factor f : (1) it falls within a fairly narrow range (e.g., near 0.3) for most ULXs, or (2) it varies from source to source or temporally for individual sources. In the first instance, the entire luminosity functions that we generate could be shifted downward in luminosity such that, e.g., the peak of the luminosity function for model B drops from 2×10^{39} ergs s⁻¹ to 6×10^{38} ergs s⁻¹, and the highest (and rarest) luminosity sources of 2×10^{40} ergs s⁻¹ fall to 6×10^{39} ergs s⁻¹. By contrast, in the second case, f varies from low to high values (among sources or temporally) then our luminosity functions might be not be so seriously shifted to lower luminosities, but would yield fewer luminous sources overall. This, in turn, would actually help the “overproduction” problem discussed in §3. If the net result of smaller values of f is to shift our simulated luminosity functions to substantially lower luminosities, then this suggests two possibilities: (1) the basic results we have generated are correct, but then the “Begeelman factor” would have to be as high as 30 instead of 10 for black-hole accretors with masses of $10 M_\odot$, or (2) the most luminous ULXs with L_x (2–10 keV) $> 10^{40}$ ergs s⁻¹ indeed represent a different class of objects, e.g., IMBHs. More work is needed both observationally, to determine f empirically with greater certainty, and theoretically, especially regarding the photon bubble instability model to ascertain if super-Eddington factors of 30 are possible.

In this work we have not included the contributions from very luminous neutron star binaries (e.g., HMXBs resembling SMC X-1 and LMC X-4). Such systems are likely to be very short lived (e.g., 10^5 yr; see e.g., Levine et al. 1991; 1993; 2000) due to the tidal interactions that drive the Roche lobe rapidly through the atmosphere of the primary. However, such neutron star binaries are much easier to form than black-hole binaries, and therefore their contributions to the luminosity function between 10^{37} and 5×10^{38} ergs s⁻¹ should be substantial. In any study attempting to compute the entire luminosity function, the luminous neutron star systems clearly need to be included (e.g., Belczynski et al. 2004). The intention of the present study, however, was limited to evaluating the contribution of stellar-mass black-hole binaries to the ULX population.

One further caveat is in order with regard to the success of our model for the ULXs. Most of the ULXs that we generate in our population synthesis have high-mass donors and are not transients. By contrast, many of the black-hole binaries discovered and studied in our Galaxy are transients whose time-averaged mass-transfer rate is well below Eddington and whose companions are rather low in mass (i.e., $< 1 M_\odot$) (see, e.g., McClintock & Remillard 2004). This apparent discrepancy between the two populations was discussed in PRH, and hinges on the fact that it is difficult, in the context of the present model, to produce black hole binaries with low initial donor masses. This problem arises due to the fact that a secondary of $< 2 M_\odot$ tends to merge with the core of the massive black-hole progenitor instead of ejecting the common envelope. Also, as demonstrated in PRH, black-hole binaries with initial donor masses $> 2 M_\odot$

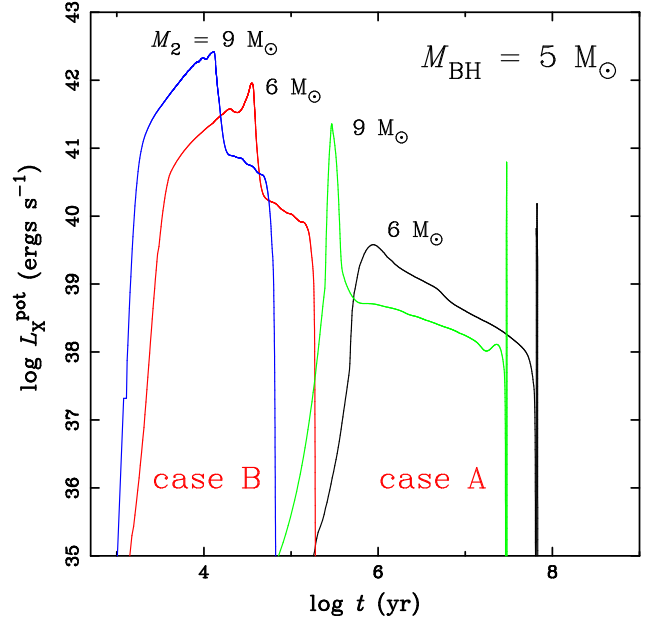


Figure 11. Potential X-ray luminosities as a function of time since the beginning of mass transfer (offset by 10^3 yr for clarity) for 4 black-hole X-ray binary evolution sequences. Each color corresponds to a different mass or evolutionary state of the donor star when mass transfer commences (as indicated). In all cases the initial mass of the black hole is $5 M_\odot$. The black and red curves are for donor stars with initial masses of $6 M_\odot$, while the green and blue curves are for donor stars with initial masses of $9 M_\odot$. For the black and green curves the donor star commences mass transfer in the middle of the main sequence (case A mass transfer). The red and blue curves correspond to the case where the donor star has evolved off the main sequence and traverses the Hertzsprung gap at the start of mass transfer (early case B mass transfer). In all four calculations, thermal timescale phases last of order 10^5 yr. Since these involve somewhat lower-mass donor stars than the main contributors to our ULX candidates, they may be more common, which can compensate somewhat for the shorter duration of the high mass transfer rate episodes.

can evolve into the type of compact systems often seen in the Galaxy but only if there is a significant source of systematic orbital angular momentum loss, e.g., magnetic braking, which has been assumed not to operate in stars with radiative outer envelopes (Parker 1955; Pylyser & Savonije 1988). We note, however, that there is a subset of stars with radiative envelopes, the Ap/Bp stars, with masses up to $3 M_\odot$ that have strong magnetic fields (> 10 kG) and long rotation periods (e.g., Hubrig et al. 2000). While the origin of the large magnetic fields in these stars and their relation to the rotation periods are presently not understood, their very existence may suggest that there could be a subset of stars with radiative envelopes where magnetic braking is operative. This is clearly a problem that warrants further consideration and modeling.

King et al. (2001) discuss the possible importance of thermal timescale mass transfer (see, e.g., PRH) onto black holes as the driver of high rates of mass transfer in ULXs. We note, however, that most ULXs in our simulations are binaries where mass transfer is driven by the nuclear evolution of the massive donor, most commonly hydrogen burning in the

core, but in a fraction of systems ($< 5\%$) by hydrogen shell burning as the donor star ascends the giant branch. Even higher mass-transfer rates can indeed be attained during phases where the secondary is out of thermal equilibrium, either during thermal timescale mass transfer or when the secondary moves across the Hertzsprung gap (so-called early case B mass transfer). However, since the lifetimes of these phases are typically several orders of magnitude shorter than the phases where mass transfer is driven by the nuclear evolution, few ULXs are expected to be found in this phase (see the dashed curve in Fig. 3)³. To illustrate this further we have done some additional binary calculations, shown in Fig. 11, for secondaries with initial masses of 6 and 9 M_{\odot} , respectively, in two evolutionary phases: in the middle of the main sequence (case A) and just after the secondary has left the main sequence and started to move across the Hertzsprung gap (early case B). In all calculations, the initial mass of the black hole was taken to be 5 M_{\odot} . In the 6 M_{\odot} case A sequence, the secondary always remains in thermal equilibrium and mass-transfer is entirely driven by the nuclear evolution of the core. For about 10^7 yr its potential X-ray luminosity (just) exceeds 10^{39} ergs s^{-1} and may be classified as a ULX during this phase. In contrast, the 9 M_{\odot} case A sequence experiences a phase of rapid, thermal timescale transfer, lasting $\sim 2 \times 10^5$ yr. During this phase the potential X-ray luminosity reaches a peak exceeding 10^{41} ergs s^{-1} . After the thermal timescale phase, mass transfer continues but now on a nuclear timescale for the next 3×10^7 yr at a rate that is not sufficient to power a ULX. Both case A systems appear as ULXs again as they ascend the giant branch where their evolution is driven by hydrogen shell burning. In the case B sequences, where mass transfer is driven by the thermal timescale evolution of the secondary across the Hertzsprung gap, the mass-transfer phases last only 10^5 yr, but reach peak mass-transfer rates of 10^{-4} and $8 \times 10^{-4} M_{\odot} \text{ yr}^{-1}$ for the 6 and 9 M_{\odot} sequences, respectively, and corresponding peak potential X-ray luminosities of order and above 10^{42} ergs s^{-1} . Note that in these latter sequences, the mass-transfer rates, and hence potential X-ray luminosities, drop by 1.5 orders of magnitude after the mass-ratio has been reversed and the orbit starts to expand rapidly. During this latter phase, the potential X-ray luminosities remain in the ULX regime, but decrease gradually (the moderately sloping portions of the curves in Fig. 11).

These sequences (Fig. 11) demonstrate that during thermal timescale mass-transfer phases, very high mass-transfer rates are attained, providing potentially enough fuel to power even the most luminous ULXs, but that the duration of these phases, which obviously scales as the inverse of the characteristic mass transfer rate, is short compared to the duration of phases where mass transfer is driven by the nuclear evolution of the secondary. A compensating factor is that lower-mass secondaries can in principle produce mass-transfer rates in the ULX regime during thermal timescale phases (onto low-mass black holes) that they could not oth-

erwise do during the nuclear-driven phases. This effect may somewhat, but not drastically increase the relative number of thermal timescale systems compared to nuclear timescale systems.

Transient source behavior, due to the thermal ionization disk instability (e.g., van Paradijs 1996; King, Kolb, & Burderi 1996; Dubus, Hamoury, & Lasota 2001) has been invoked as a way of producing higher mass transfer rates, albeit only for concomitantly reduced fractional times of the total binary mass transfer phase. We have found that when we include transient source behavior, which occurs predominantly in systems with lower average luminosity (e.g., $< 10^{37}$ ergs s^{-1}), there is essentially no change in the luminosity function for times < 100 Myr; thereafter, there is a modest enhancement of high- L_x sources due to transient source behavior, but the bulk of these objects have luminosities $< 5 \times 10^{38}$ ergs s^{-1} (see Fig. 4, panel [d]).

The giant phase of the donor star is also a natural mechanism to consider for driving mass transfer rates that could enhance the ULX population. The mass transfer phase driven by the ascent of the donor up the giant branch is dramatically evident in Fig. 1 as "spikes" in L_x near the end of the evolution. Indeed the mass transfer rate increases during this phase by 1–2 orders of magnitude. However, this phase is relatively short lived and tends not to contribute dramatically to the population of ULXs. Fig. 4 shows the integrated contribution of the giant branch phase of mass transfer to the ULX population – these are seen as a red ridge lying

1.5 orders of magnitude above the peak in the luminosity function for times > 15 Myr. One could argue that in galaxies where the Chandra sensitivity limit is 10^{39} ergs s^{-1} , these (giant branch) sources would be the only ones visible at $t_{\text{ev}} > 15$ Myr. This is true, but then the issue arises as to what absolute numbers of sources are predicted. As can be seen from Fig. 6 the contributions from giant-branch donor sources do show up as a modestly significant feature for $L_x > 10^{40}$ ergs s^{-1} at 30 Myr.

Our models also have some predictive power concerning the optical appearance of the ULX black-hole binaries. We have computed tracks for our binary evolution models in the HR diagram, taking into account both the contribution from the donor star and the accretion disk. Light from the disk, in turn, results from reprocessing of X-radiation and from viscous heating. We computed the effective temperature of the disk as a function of radius, r , from the following simple expression that we derived:

$$T(r) = \frac{L_x}{4 r_{\text{in}}^2} \left(\frac{h}{2} \right)^{1/4} x^{1/2} (1 - \alpha) + \frac{3}{2} x^{3/4} \dot{m}_{\text{in}}^{1/4}; \quad (7)$$

where x is the radial distance in units of r_{in} , the inner radius of the disk, α is the X-ray albedo of the disk (which we take to be 0.7), and \dot{m}_{in} is defined by $\dot{m}_{\text{in}} = \dot{m}_{\text{ax}} (r_{\text{in}}/r_{\text{ax}})^{2/7}$, where, in turn, \dot{m}_{ax} is the half thickness of the disk, h , at r_{ax} , in units of r_{ax} . In this formulation $h(r) = r^{9/7} \dot{m}_{\text{ax}}^{2/7}$, and we take $\dot{m}_{\text{ax}} = 0.1$ as an illustrative value corresponding to a full angular thickness of the disk equal to $\sim 12^\circ$. For the disk-heating problem only, we have taken the inner edge of the accretion disk to be at $6GM_{\text{BH}}/c^2$ regardless of the spin of the black hole, and we have neglected the factor

³ This is generally true for mass transfer from a more massive star to a less massive star and, as is well known, explains, e.g., the paucity of Lyrae systems compared to Algol-type systems, believed to be their descendants (for a general discussion, see Paczynski 1971).

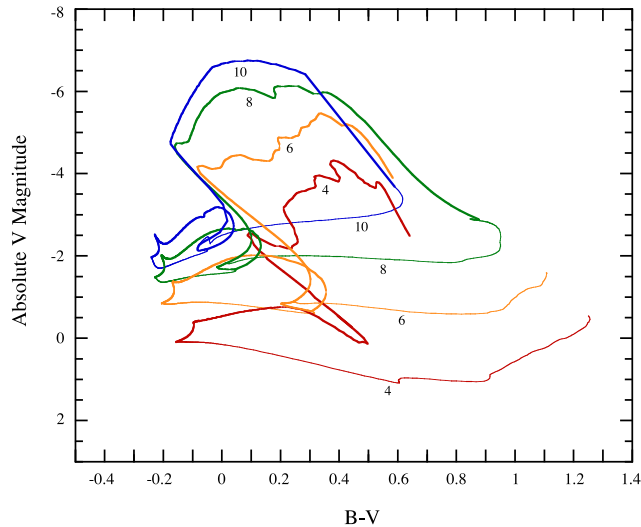


Figure 12. Evolution tracks in the HR diagram are shown for 4 of our models; these are for donors stars that had initial masses of 4, 6, 8, and 10 M_{\odot} and were on the zero-age main sequence at the start of mass transfer. Each binary system is represented by two different evolution tracks; the thin curve is the contribution from the donor star alone, while the thicker curve (of the same color) describes the track for the total system light (both disk and donor star).

1 $P_{\text{in}} = r$ found in the Shakura & Sunyaev (1973) solutions. This latter approximation affects only the x^3 term which, in any case, contributes little to the optical flux from the disk. The contributions to the B and V bands from the donor stars were estimated from their bolometric magnitude and effective temperature using conversion factors taken from Reed (1998).

Illustrative results for 4 evolution tracks in the HR diagram are shown in Fig. 12; these are for donors stars that had initial masses of 4, 6, 8, and 10 M_{\odot} and were on the zero-age main sequence at the start of mass transfer. Each binary system is represented by two different evolution tracks in the HR diagram; the thin curve is the contribution from the donor star alone, while the thicker curve (of the same color) describes the track for the total system light (both disk and donor star). In each case, it is clear that during the early part of the binary evolution where the donor star is still on the main sequence, the contribution from the heated accretion disk leads to a brighter optical counterpart in the V band by about 1 magnitude. However, during the short-lived giant branch phase, when the X-ray luminosity is very much larger, the V-band magnitudes are enhanced by 4 magnitudes and the system colors are considerably bluer. Thus, we conclude that there is a substantial contribution to both the color and magnitude of the optical counterparts of the black-hole ULXs from the accretion disk. Moreover, we note that the contribution of the donor star to the optical light of the system may be considerably less than might be expected from a star of the same initial mass, especially if the mass transfer commences early in the evolution of the donor star. These facts should be taken into account by observers trying to characterize the "donor star" from its location in an HR diagram (M. Pakull, private communication).

Finally, we briefly discuss the issue of ULXs in elliptical galaxies (e.g., Angelini, Loewenstein, & Mushotzky 2001; Colbert & Ptak 2002; Jettam et al. 2003; Ptak & Colbert 2004). The presence of true ULXs with certified X-ray luminosities exceeding 10^{39} ergs s^{-1} would be very difficult to explain within the context of our black hole binary model unless the elliptical galaxy had a recent (e.g., $< 3 \times 10^8$ yr) merger and star formation cycle. Recently Irwin, Bregman, & Athey (2004) have shown, from a sample of 28 elliptical and S0 galaxies observed with Chandra, that the number of sources with $L_x > 2 \times 10^{39}$ ergs s^{-1} was equal to the number expected from background or foreground objects. Thus, they conclude that, with only the exception of two ULXs in globular clusters within NGC 1399, ULXs "are generally not found within old stellar systems". Nonetheless, the ULXs found in early-type galaxies with $10^{39} < L_x < 2 \times 10^{39}$ ergs s^{-1} are not naturally explained within the context of our model.

In summary, our calculations indicate that with a plausible set of assumptions, a majority of the ULXs with $L_x < 10^{40}$ ergs s^{-1} in spiral galaxies can be understood in terms of binary systems containing stellar-mass black holes. The systems can be evolved theoretically from the primordial binary phase through the ULX phase and the absolute numbers of such systems in the populations that are computed are in agreement with the observations to order-of-magnitude accuracy. By contrast, the same claim cannot yet be made for the model of ULXs that invokes intermediate-mass black holes. Such a model, of course, has the advantages that (1) the Eddington limit presents no difficulties, and (2) the spectra of some of the ULXs which exhibit low inner-disk temperatures (see, e.g., Miller et al. 2003; Cropper et al. 2004) may be a natural consequence of more massive black holes. However, in the context of the IMBH model, ideas as to how such objects are formed, acquire binary companions, and are "fed" at the requisite accretion rates are only just beginning to be explored (see, e.g., Portegies Zwart et al. 2004; Portegies Zwart, Dewi, & Maccarone 2004; and references therein).

ACKNOWLEDGEMENTS

We thank Ed Colbert, Miriam Krauss, Ron Remillard, and Tim Roberts for helpful discussions. One of us (SR) acknowledges support from NASA RXTE Grant NAS5-30612. Ph.P. thanks the Chandra subcontract to MIT for partial support during his visit to MIT. EP was supported by NASA and Chandra Postdoctoral Fellowship Program through grant number PF2-30024.

REFERENCES

- Angelini, L., Loewenstein, M., & Mushotzky, R. F. 2001, *ApJ*, 557, L35.
- Bardeen, J. M. 1970, *Nature*, 226, 64.
- Begelman, M. 2002, *ApJ*, 568, 97.

- Belczynski, K., Kalogera, V., Zezas, A., & Fabbiano, G. 2004, *ApJ*, 601, L147.
- Cannizzo, J.K., Ghosh, P., & Wheeler, J.C. 1982, *ApJ*, 260, L83.
- Cappellaro, E., Evans, R., & Turatto, M. 1999, *A & A*, 351, 459.
- Colbert, E., & Mushotzky, R. 1999, *ApJ*, 519, 89.
- Colbert, E., & Ptak, A.F. 2002, *ApJS*, 143, 25.
- Colbert, E.J.M., & Miller, M.C. 2004, talk at the Tenth Marcel Grossmann Meeting on General Relativity, Rio de Janeiro, July 20-26, 2003. Proceedings edited by M. Novello, S. Perez-Berglia and R. Ruini, World Scientific, Singapore, 2004 [astro-ph/0402677].
- Cropper, M., Soria, R., Mushotzky, R.F., Wu, K., Markwardt, C.B., & Pakull, M. 2004, *MNRAS*, 349, 39.
- Dewi, J., & Tauris, T. 2000, *A & A*, 360, 1043.
- Dubus, G., Hamery, J.-M., & Lasota, J.-P. 2001, *A & A*, 373, 251.
- Fabbiano, G. 1989, *ARA & A*, 27, 87.
- Fabbiano, G., Zezas, A., & Murray, S.S. 2001, *ApJ*, 554, 1035.
- Fabbiano, G., & White, N.E. 2004, to appear in "Compact Stellar X-Ray Sources", eds. W.H.G. Lewin and M. van der Klis, (Cambridge Univ. Press: Cambridge) [astro-ph/0307077].
- Fryer, C.L., & Kalogera, V. 2001, *ApJ*, 554, 548.
- Gao, Y., Wang, D.Q., Appleton, P.N., & Lucas, R.A. 2003, *ApJ*, 596, L171.
- Gilfanov, M., Grimm, H.-J., & Sunyaev, R. 2004, *MNRAS*, 347, 57.
- Greiner, J., Cuby, J.G., & McCaughrean, M.J. 2001, *Nature*, 414, 522.
- Greiner, J., Morgan, E., & Remillard 1996, *ApJ*, 473, L107.
- Hemquist, L., & Weil, M. 1993, *MNRAS*, 261, 804.
- Howell, S.B., Nelson, L.A., & Rappaport, S. 2001, *ApJ*, 550, 897.
- Hubrig, S., North, P., & Mathys, G. 2000, *ApJ*, 539, 352.
- Irwig, J.A., Athey, A.E., & Bregman, J.N. 2003, *ApJ*, 587, 356.
- Irwig, J.A., Bregman, J.N., & Athey, A.E. 2004, *ApJ*, 601, L143.
- Jeltema, T.E., Canizares, C.R., Buote, D.A., & Garmire, G.P. 2003, *ApJ*, 585, 756.
- King, A.R. 2002, *MNRAS*, 335, L13.
- King, A.R., & Kolb, U. 1999, *MNRAS*, 305, 654.
- King, A.R., Kolb, U., & Burderi, L. 1996, *ApJ*, 464, L127.
- King, A.R., Davies, M.B., Ward, M.J., Fabbiano, G., & Elvis, M. 2001, *ApJ*, 552, L109.
- Kording, E., Falcke, H., & Marko, S. 2002, *A & A*, 382, L13.
- Kroupa, P., Tout, C.A., & Gilmore, G. 1993, *MNRAS*, 262, 545.
- Lasota, J.-P. 2001, *New AR*, 45, 449.
- Lee, C.-H., et al. 2002, *ApJ*, 575, 996.
- Levine, A., Rappaport, S., Putney, A., Corbet, R., & Nagase, F. 1991, *ApJ*, 381, 101.
- Levine, A., Rappaport, S., Deeter, J.E., Boynton, P.E., Nagase, F. 1993, *ApJ*, 410, 328.
- Levine, A., Rappaport, S., & Zojcheski, G. 2000, *ApJ*, 541, 194.
- Malakshin, K., et al. 2000, *ApJ*, 535, 632.
- McIntock, J.E., & Remillard, R. 2004, to appear in "Compact Stellar X-Ray Sources", eds. W.H.G. Lewin and M. van der Klis, (Cambridge Univ. Press: Cambridge) [astro-ph/0306213].
- Miller, G.E., & Scalzo, J.M. 1979, *ApJS*, 41, 513.
- Miller, J.M., Fabbiano, G., Miller, M.C., & Fabian, A.C. 2003, *ApJ*, 585, L37.
- Miller, J.M., Fabian, A.C., & Miller, M.C. 2004a, *ApJ*, 607, 931.
- Miller, J.M., Fabian, A.C., & Miller, M.C. 2004b, *ApJ*, in press [astro-ph/0406656].
- Nelms, G., & van den Heuvel, E.P.J. 2001, *A & A*, 376, 950.
- Paczynski, B. 1971, *ARA & A*, 9, 183.
- Pakull, M., & Mirioni, L. 2003, *RMxAC*, 15, 197.
- Parker, E.N. 1955, *ApJ*, 122, 293.
- Pfahl, E., Rappaport, S., & Podsiadlowski, Ph. 2003, *ApJ*, 597, 1036.
- Podsiadlowski, Ph., Rappaport, S., & Pfahl, E. 2002, *ApJ*, 565, 1107.
- Podsiadlowski, Ph., Rappaport, S., & Han, Z. 2003, *MNRAS*, 341, 385 [PRH].
- Portegies Zwart, S., Verbunt, F., & Ergm, E. 1997, *A & A*, 321, 207.
- Portegies Zwart, S., Baumgardt, H., Hut, P., Makino, J., & McMillan, S.L.W. 2004, *Nature*, 428, 724.
- Portegies Zwart S.F., Dewi, J., & Accarone, T. 2004, submitted to *MNRAS*.
- Ptak, A., & Colbert, E. 2004, *ApJ*, in press [astro-ph/0401525].
- Pylser, E., & Savonije, G.J. 1988, *A & A*, 191, 57.
- Reed, C. 1998, *J. R. A. S. Canada*, 92, 36.
- Ranalli, P., Comastri, A., & Seti, G. 2003, *A & A*, 399, 39.
- Roberts, T., & Warwick, R. 2000, *MNRAS*, 315, 98.
- Ruszkowski, M., & Begelman, M.C. 2003, *ApJ*, 586, 384.
- Salpeter, E.E. 1955, *ApJ*, 121, 161.
- Shakura, N.I., & Sunyaev, R.A. 1973, *A & A*, 24, 337.
- Tanaka, Y., & Lewin, W.H.G. 1995, *X-Ray Binaries*, eds. W.H.G. Lewin, J. van Paradijs, & E.P.J. van den Heuvel (Cambridge: Cambridge University Press), p. 126.
- van Paradijs, J. 1996, *ApJ*, 464, L139.
- Voss, R., & Tauris, T.M. 2003, *MNRAS*, 342, 1169.
- Webbink, R. 1985, in *Interacting Binary Stars*, ed. J.E. Pingle & R.A. Wade (Cambridge: Cambridge Univ. Press), 39.
- Wolter, A., & Trinchieri, G. 2003, *MSAL*, 73, 23.
- Wolter, A., & Trinchieri, G. 2004, submitted to *A & A* [astro-ph/0407446].
- Zezas, A., & Fabbiano, G. 2002, *ApJ*, 577, 726.
- Zezas, A., Fabbiano, G., Rots, A.H., & Murray, S.S. 2002, *ApJ*, 577, 710.